International Journal of Fatigue 159 (2022) 106798

Contents lists available at ScienceDirect

International Journal of Fatigue

journal homepage: www.elsevier.com/locate/ijfatigue

Mechanical fatigue of biodegradable polymers: A study on polylactic acid (PLA), polybutylene succinate (PBS) and polybutylene adipate terephthalate (PBAT)

Jian Zhang [a], Valerian Hirschberg [b], Denis Rodrigue [a,*]

[a] Department of Chemical Engineering and CERMA, Université Laval, 1065 Avenue de la Médecine, Quebec G1V 0A6, Canada
[b] Institute for Chemical Technology and Polymer Chemistry, Karlsruhe Institute of Technology (KIT), Engesserstraße 18, Karlsruhe 76131, Germany

ARTICLE INFO

Keywords:
Fatigue
PLA
PBS
PBAT
Fourier transform
Non-linear analysis

ABSTRACT

The fatigue behavior of three biodegradable polymers, PLA (polylactic acid), PBS (polybutylene succinate) and PBAT (polybutylene adipate terephthalate) was determined under cyclic tension/tension loading in strain-controlled measurements. Stress response and surface temperature were recorded and analyzed to compare their behavior and evolution with on-going fatigue. The stress was decomposed into linear and nonlinear contributions by Fourier transform (FT) analysis and higher harmonics were correlated with fatigue. The surface temperature variation is analyzed as a function of the strain amplitude and compared for these materials during fatigue. The relative even ($I_{2/1}$) and odd ($I_{3/1}$) higher harmonics (ratio between the n^{th} harmonic to the fundamental one ($I_{n/1}$)) in the stress response were found to be good criteria for fatigue characterization. The cumulative nonlinearity parameter ($^{n}Q_f$), defined as the (cycle number) integral of the relative higher harmonic, normalized to the strain amplitude with an exponent of $n - 1$, was found to be the best criterion to quantify mechanical fatigue and predict fatigue lifetime.

1. Introduction

Mechanical fatigue occurs when a material is exposed to cyclic loading, which is related to its intrinsic mechanical properties and structure. Usually, the fatigue life of thermoplastics, such as high-density polyethylene (HDPE), polyamide 6 (PA6), ultra high molecular weight polyethylene (UHMWPE) and polypropylene (PP), polystyrene (PS) decreases with increasing strain amplitude [1–4]. Increasing the strain ratio (minimum strain divided by maximum strain) from 0.1 to 0.5 was found to decrease the fatigue resistance (fatigue life = number of cycle to failure, N_f) of polymethylmethacrylate (PMMA) and PS by up to one order of magnitude [5]. A recent study also reported an important decrease of the fatigue resistance when low density polyethylene (LDPE) was exposed to ultraviolet (UV) irradiation [6]. But increasing the molecular weight can improve the fatigue performance under fixed testing conditions [2,3]. Although several investigations studied the fatigue behavior of a broad range of thermoplastics, information on the fatigue performance of biodegradable polymers is almost inexistent in the current literature even if these materials are gaining more interest for different applications, especially in packaging. With respect to sustainability, *carbon neutral* or *net-zero* concepts became the new mantra in this century to limit global warming below 2 °C, but preferably to 1.5 °C above pre-industrial levels [7]. For example, greenhouse gas (GHG) emissions from plastics is expected to reach 15% of the global carbon budget by 2050 [8]. Therefore, minimizing the carbon footprint from plastics is an essential part of GHG mitigation. However, a very limited amount of plastics waste is recycled (around 9% in Canada [9]) which is detrimental to achieve the target [10]. Recent studies indicated that integrating recycling and replacing fossil fuel-based plastics by biodegradable/compostable/biobased plastics is a promising approach to reduce GHG emissions from plastics [10,11].

One option is to replace petroleum-based polymers by biosourced/biodegradable polymers with or without natural fiber reinforcement. This transition implies replacing environmental unfriendly (petro-based) plastics by biodegradable/compostable (preferably bio-based) ones, like PLA (polylactic acid), PBS (polybutylene succinate) and PBAT (polybutylene adipate terephthalate), for applications, such as packaging, automotive, consumer goods, healthcare, etc. Furthermore, these polymers can be filled with biobased particles (lignocellulosic fibers for example) to further improve their mechanical performances.

One example is cellulose nanofibers, which can improve the

* Corresponding author.
E-mail address: denis.rodrigue@gch.ulaval.ca (D. Rodrigue).

https://doi.org/10.1016/j.ijfatigue.2022.106798
Received 17 November 2021; Received in revised form 7 January 2022; Accepted 11 February 2022
Available online 16 February 2022

Nomenclature

$d(F/F_0)/dN$	loading degradation rate
$dI_{3/1}/dN$	rate of change of $I_{3/1}$
E'	storage modulus
E''	loss modulus
F	test frequency
F	maximum force during cyclic loadings
F_0	initial value of F from the first loading
I_i	fundamental harmonic
$I_{2/1}$	ratio of the second harmonic normalized by the fundamental
$I_{3/1}$	ratio of the third harmonic normalized by the fundamental
${}^nQ$	$I_{n/1}/\varepsilon_0^{n-1}$
${}^nQ_f$	cumulative nonlinearity
R	strain ratio, $\varepsilon_{min}/\varepsilon_{max}$
tan δ	loss factor
T_a	ambient temperature
T_g	glass transition temperature
W_{diss}	dissipate energy

Greek letters

ΔT	surface temperature rise
ΔT_{max}	maximum surface temperature rise
δ_n	phase angle of the nth harmonics
ε_0	strain amplitude
σ	stress
$\varnothing$	phase angle
ϕ	phase shift
ω_1, ω	angular frequency of the deformation

mechanical stiffness, strength and elastic modulus of polymers [12]. Blending CNC with PBS was found to increase the Young's modulus at the cost of elongation at break. Higher yield strength was observed when the CNC content was below 3 wt% [13]. Addition of reinforcement based on biomass to PBS was reported to increase the tensile properties [14–20], while some natural fillers (lignin, starch, etc.) decreased them [21–23]. The mechanical properties of PBAT can also be improved by producing composites. However, the main challenge is always the compatibility between nonpolar/hydrophobic matrices with polar/hydrophilic natural fillers [24,25]. To overcome this issue, surface modification of the fillers must be conducted to improve the interaction with the matrix. Blending surface modified CNC [26–28], nanofibrillated cellulose [29], and organoclay [30] can improve the elastic modulus and tensile strength. For example, 6 wt% acetylated cellulose nanocrystals (CNC) into PLA was shown to improve the tensile strength by 61% due to good interactions (high interfacial adhesion) with the neat PLA [31]. However, lower tensile strength (10–20%) and elongation at break (11–17%) of PLA/nanoclay (0–5 %wt.) composite was observed [32].

For specific applications with a long service life, it is essential to determine their long terms properties/endurance. For design purposes, studies dedicated to mechanical properties prediction must be done [33]. However, very limited information is available on the fatigue behavior of biodegradable polymers (alone or as the matrix of composites). Most of the data available are from additively manufactured (AM) samples based on PLA. For example, it was reported that the raster angle during printing highly affected the fatigue lifetime of unnotched sample and 45° was identified as providing the optimal performance [34]. However, Bzeh et al. suggested that 3D printed PLA can be treated as a homogenous and isotropic material from a fatigue point of view [35]. For notched PLA specimens, an increase of the notch angle decreased the fatigue resistance as the cracks propagated along the filaments orientation [36]. Cicero et al. found that for notched specimen (localized defect), the optimal orientations were 30°/-60° and 45°/-45° leading to higher fracture resistance [37]. But the measuring conditions also affect the final results. For example, Vanaei et al. reported that increasing the loading amplitude (5–55 MPa) and frequency (1–80 Hz) highly reduced the fatigue lifetime of 3D printed PLA [38].

Although some investigations provided useful information on the mechanical properties of biodegradable polymers, they mostly focused on the mechanical properties under static and quasi-static testing. No comprehensive overview or comparison of the fatigue properties of these polymers can be found in the literature. Therefore, more research must be done to fully characterize the fatigue behavior of these polymers as a systematic characterization of their fatigue behavior is still an uncharted territory. To provide a broader overview, this work investigates and compares the mechanical fatigue behavior of three commercially available polymers: PBS, PBAT and PLA. For example, PLA is an interesting material applied in 3D printing and PBS is considered as a suitable biodegradable replacement of polypropylene. Furthermore, their scope of application is still growing due to their biodegradability. But first, the main theories and parameters are described to relate with the results presented. But first, the main theories and parameters are described to relate with the results presented.

2. Nonlinear theory based on FT analysis

For sinusoidal strain-controlled fatigue tests, the stress response of polymers becomes nonlinear under sufficiently large oscillatory strains [5]. In this case, the stress response is no longer in phase with the input strain and the linear parameters partly loose their meaning as a material property [39]. However, this nonlinear behavior can be quantified via Fourier transform (FT) with high sensitivity by separately analyzing each higher harmonics in the frequency domain from their response in the time domain [40–42]. This transformation (time to frequency) can be done via FT and quantified by a limited number of frequency as $I(\omega_1)$, $I(2\omega_1)$, $I(3\omega_1)$, etc., while the remaining points of the truncated spectra are assumed to be non-periodic (noise) as a first approximation [5]. Thus, the stress in the frequency domain can be expressed as [43]:

$$\sigma = I_1 e^{i\omega t+\delta_1} + I_2 e^{2i\omega t+\delta_2} + I_3 e^{3i\omega t+3} + I_4 e^{4i\omega t+\delta_4} + I_5 e^{5i\omega t+\delta_5} + \cdots \quad (1)$$

More details on FT analysis of mechanical signals can be found in the works of Hirschberg et al. [1–3,5,39,42,43] and Hyun et al. [40,44]. The higher harmonics (I_n, $n > 2$) are generally normalized by the fundamental one (I_1) and denoted as $I_{n/1}$. With this normalization, the intensity of each higher harmonics for different materials or testing conditions can be easily compared [5].

To further quantify nonlinear parameters as fatigue criteria, the intensities ($I_{n/1}$, $n > 1$) can be normalized by ${\varepsilon_0}^m$ and the ratio is defined as the Q parameter [3]. Since higher harmonics depend on the strain amplitude via power-law functions with an exponent $m = n - 1$, the Q parameters are calculated as [45,46]:

$${}^nQ = \frac{I_{n/1}}{\varepsilon_0^{n-1}} \quad (2)$$

The cumulative nonlinearity ${}^nQ_f$ is obtained by integration of ${}^nQ$ from the beginning of a test until specimen failure as:

$${}^nQ_f = \int_0^{N_f} Q dN \quad (3)$$

where N_f is the number of cycles for failure. As proposed by Hirschberg et al. [3], the ${}^3Q_f$ parameter can provide better statistics to quantify fatigue since it is independent of the measurement conditions and only

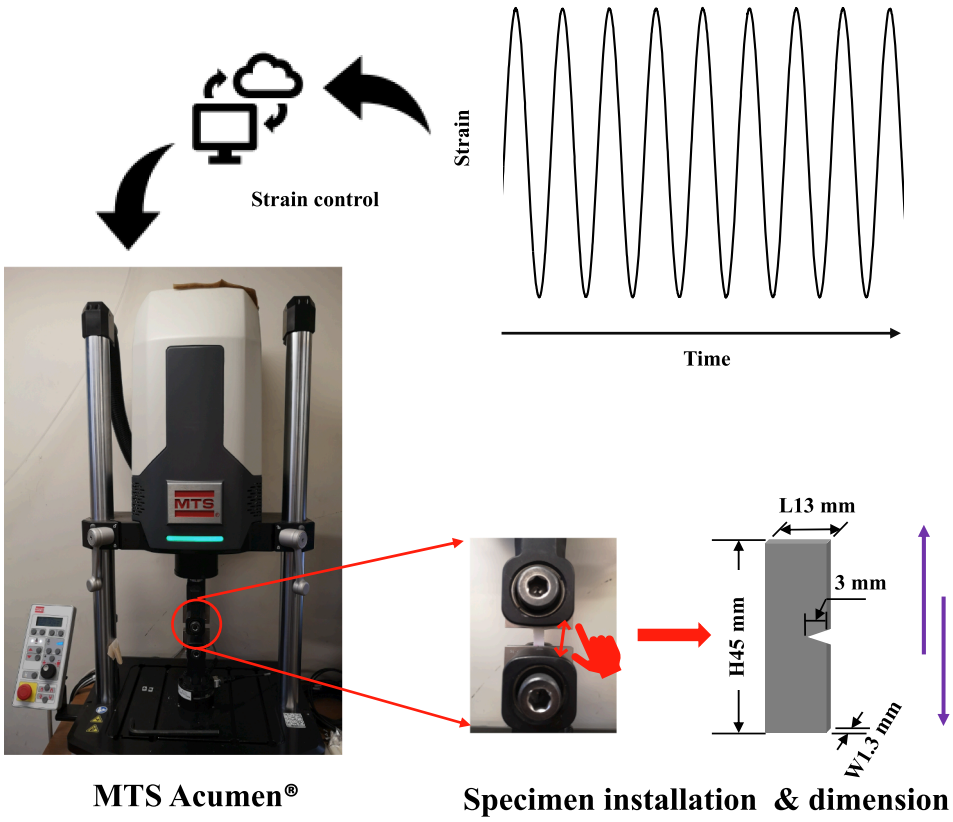

Fig. 1. Schematic diagram of the fatigue characterization set-up and conditions.

Table 1
Material properties and molding conditions.

Material properties			
Resin	PLA (2003D)	PBS (FZ71)	PBAT(TH801T)
Density, g/cm^3	1.25	1.26	1.21
Melting point, °C	130–180 [47,48]	115 [47]	110–122 [49]
Glass transition, °C	50–80 [48]	−28.5 [50]	−33 [49,51]
Molding conditions			
Temperature, °C	180 [52]	160 [51]	140
Pressure, MPa	0.05 [53]	0.05 [53]	0.05 [53]
Time, min	20	20	20

related to fatigue.

Here, the second ($I_{2/1}$) and third ($I_{3/1}$) higher harmonics were selected to quantify the cumulative nonlinearity as ^2Q_f and ^3Q_f, respectively. Therefore, a quantitative comparison of the nonlinear parameters is investigated under dynamic tension–tension fatigue testing analyzed via FT characterization.

3. Experimental details

3.1. Materials

Three biodegradable polymers were selected to compare their fatigue behavior: PLA (2003D, NatureWorks), PBS (FZ71, Mitsubishi) and PBAT (TH801T, TunHe). The specimens were compression molded into a notched rectangular mold with dimensions of: length = 13 mm, width = 45 mm and thickness = 1.3 mm as shown in Fig. 1. The V-notch was in the middle with an angle of 45°. More details about the materials and molding conditions can be found in Table 1.

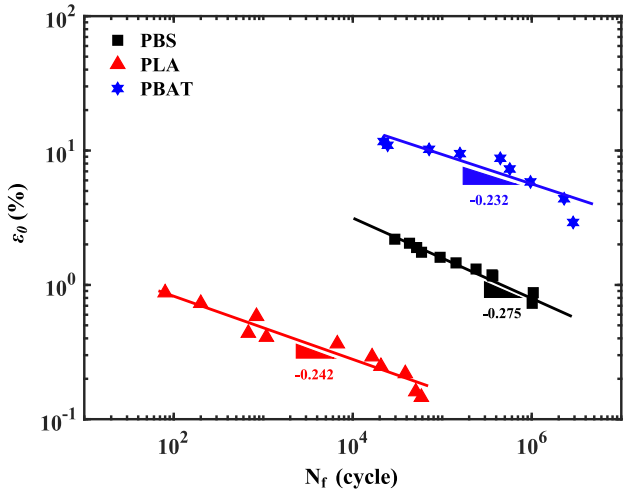

Fig. 2. Strain-life curves for PBS (■), PBAT (∗) and PLA (▲): strain amplitude (ε_0) as a function of the number of cycles to failure (N_f).

3.2. Dynamic fatigue testing & thermal characterization

The experiments were performed under sinusoidal deformation (strain controlled) on an Acumen 3 (MTS) fatigue testing setup as shown in Fig. 1. The strain amplitudes chosen are up to 50% of the strain at yield of each polymer to avoid high differences between the testing conditions. The specimens were submitted to uniaxial tension–tension oscillation at a frequency of 5 Hz and a strain ratio $R = 0.3$. To improve anti-aliasing performance and increase data resolution (reduce noise), oversampling was applied.[54] The time signals of the force and displacement were recorded by a data acquisition card with a sampling

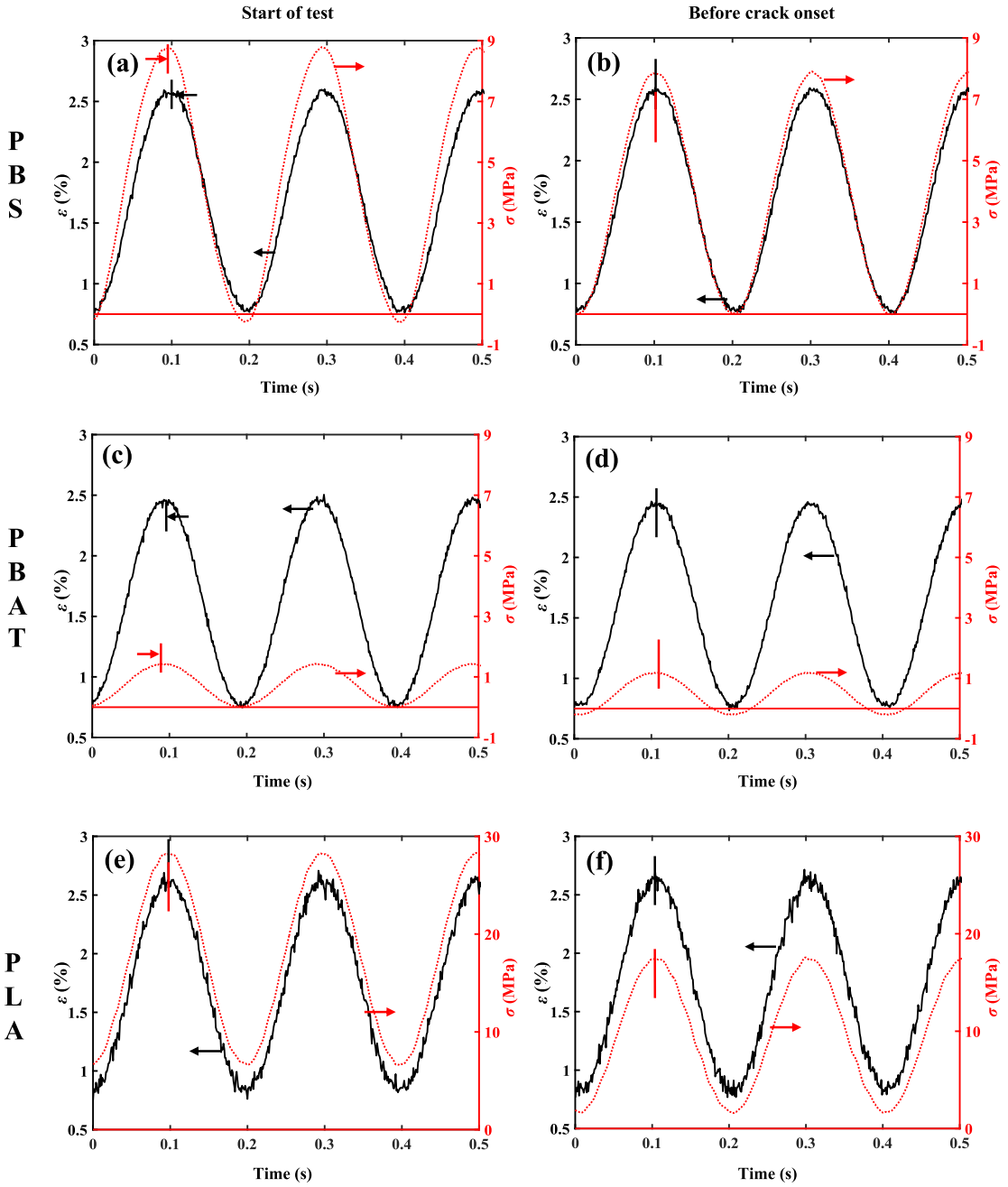

Fig. 3. Cyclic loading of the three materials at $\varepsilon_0 = 0.875\%$ and $f = 5$ Hz: time series strain and stress response at the start of the tests for: (a) PBS, (c) PBAT, (e) PLA; time series of strain and stress response before crack onset for: (b) PBS, (d) PBAT, (f) PLA.

rate of 200 points/cycle. The experiments were conducted at ambient temperature (T_a = 23 °C) and followed by a thermal camera (FLIR ThermoVision A320) registering surface temperature of the polymers during a fatigue test with a sampling rate of 35 points/second. The materials' nonlinear mechanical properties were extracted via MATLAB code based on *Fourier* transform developed in-house.

4. Results and discussion

4.1. Fatigue characterization – Strain-life curve

The fatigue life (N_f) is correlated with the applied strain amplitude (ε_o) in Fig. 2 as strain-life curves and the results can be well fitted to a power-law relation as [2]:

$$\varepsilon_0 = AN_f^C \tag{4}$$

For all materials, the exponent C is quite similar (about $-1/4$) ranging from -0.275 to -0.232, but the prefactor A varies significantly (PLA = 2.56, PBS = 37.9, PBAT = 133.6). The fatigue resistance of brittle PLA is very limited as it is not able to sustain strain amplitudes of >1%. The toughness of ductile PBAT is the highest, resulting in the highest fatigue resistance, followed by PBS and PLA. A comparison between the mechanical properties of the three polymers can be obtained by referring to their stress–strain curves in Fig. A.1.

4.2. Analysis of the stress response

To compare the strain–stress response among the three

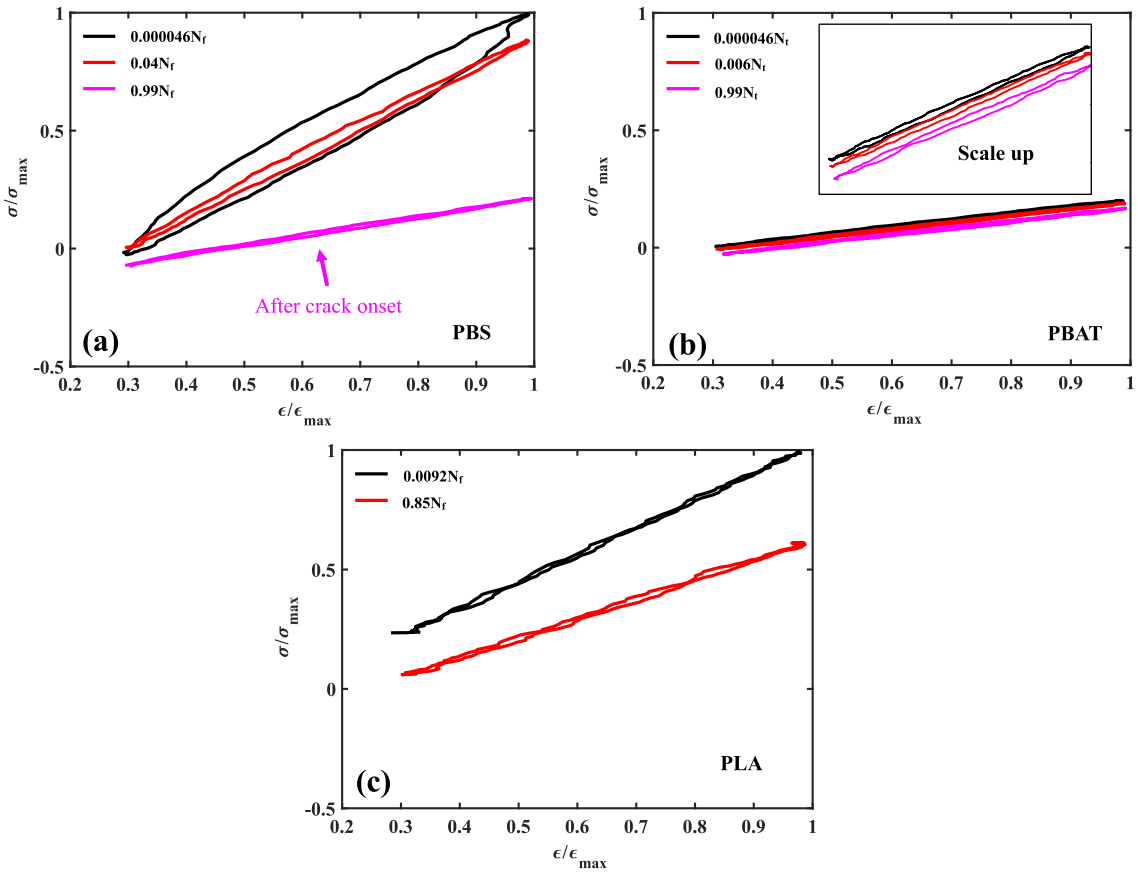

Fig. 4. Hysteresis (Lissajous) curves of different cyclic loadings during testing at $\varepsilon_0 = 0.875\%$ and $f = 5$ Hz for: (a) PBS, (b) PBAT, (c) PLA. The stress and strain were normalized by their respective maximum value. σ_{max} is the peak stress of the first cycle.

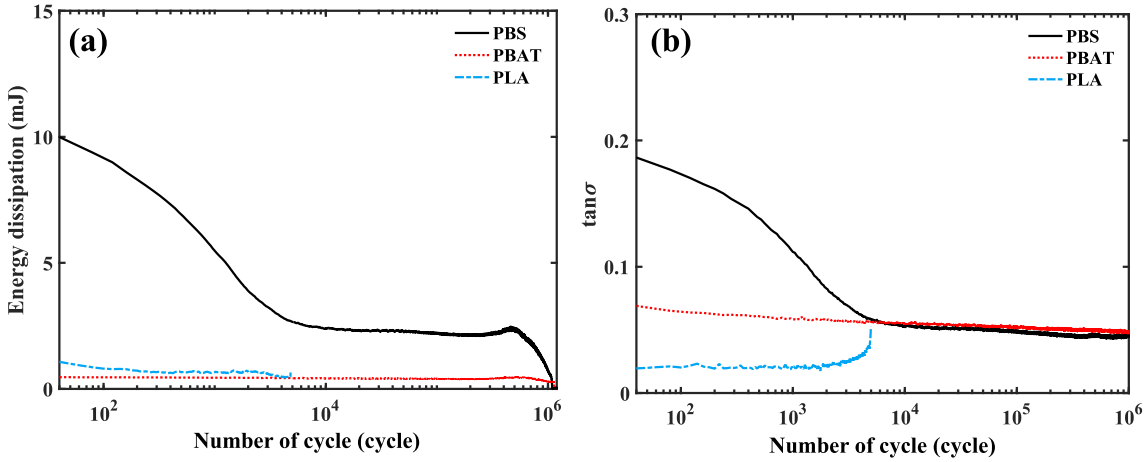

Fig. 5. Comparison of: (a) energy dissipation (W_{diss}) and (b) loss factor (tan δ) during cyclic tension–tension loading (fatigue tests) at a strain amplitude $\varepsilon_0 = 0.875\%$ and a frequency $f = 5$ Hz for PBS, PBAT and PLA.

biodegradable polymers PBS, PBAT and PLA, the time signals of the strain and stress under identical conditions ($\varepsilon_0 = 0.875\%$, $f = 5$ Hz) are presented in Fig. 3. The strain amplitude of $\varepsilon_0 = 0.875\%$ at $R = 0.3$ is the maximum ε_0 that PLA can sustain for the given specimen geometry. Interestingly, the phase shift, $\varphi(t) = \phi_{in}(t) - \phi_{out}(t)$, decreases for PBS during testing (Fig. 3a,b); i.e. the materials becomes more elastic. Here, $\phi_{in}(t)$ and $\phi_{out}(t)$ are the phase angle of the imposed sinusoidal strain signal (input) and the sinusoidal stress response (output) at a time t, respectively. However, this trend is limited for PBAT (Fig. 3c,d) and PLA (Fig. 3e,f). The difference between the input strain and out-of-phase response stress is a strong indication that PBS has a stronger viscous behavior than PBAT and PLA under the selected conditions, dissipating more heat with ongoing dynamic cycling as discussed later.

An informative parameter to assess the fatigue behavior of materials is the energy dissipation. Intrinsic self-heating and thermoelastic coupling during dynamic fatigue testing are generic fingerprints for fatigue prediction [1]. It was expected that the viscoelastic/plastic behavior of biodegradable polymers contributes to energy absorption and dissipation during dynamic loading. Fig. 4 describes the strain–-stress hysteresis loop at specific cycles. As expected, the maximum stress

Table 2
Complex, storage and loss moduli for the three polymers in the linear regime tested at $\varepsilon_0 = 0.875\%$ and $f = 5$ Hz.

Modulus	PBS	PBAT	PLA
$\|E^*\|$, MPa	22.5	4.05	40.4
E', MPa	22.5	4.04	40.3
E'', MPa	1.08	0.28	0.90
tan δ	0.048	0.069	0.022

Table 3
Cumulative nonlinearity (^2Q_f, ^3Q_f), strain amplitudes and fatigue lifetime of PBS and PBAT.

ε_0 (%)	PBS			PBAT		
	N_f (10^3 cycle)	^2Q_f (10^3)	^3Q_f (10^3)	N_f (10^3 cycle)	^2Q_f (10^3)	^3Q_f (10^3)
11.67	N.A.			22	96	291
10.21				71	232	341
8.75				445	1055	3226
7.29				568	1333	6046
5.83				967	1758	12,967
2.92				2300	1470	25,143
2.19	29	28	1679			
2.04	43	28	3892	N.A.		
1.90	51	33	5399			
1.75	58	31	5958			
1.60	94	39	9343			
1.46	142	51	13,416			
1.17	238	134	24,978			
1.31	367	120	47,342			

decreased with increasing number of cycles (N) for all materials, indicating a loss (degradation) of mechanical strength: i.e. lower modulus values. Although these observations are analyzed based on selected results, they are representative of the overall behavior over the course of the tests as fatigue is a continuous process.

The energy dissipation (W_{diss}) can be compared based on the enclosed area of the hysteresis loop (strain–stress curves). It is worth to note that PBS has the largest area compared to PBAT and PLA for the cycles before crack onset. PBAT and PLA have comparable heat dissipation, which is further quantified by integrating the force and displacement in each cycle. Fig. 5(a) presents the energy dissipation during the fatigue test up to complete fracture or to reach 10^6 cycles [1]. PBS has the highest energy dissipation at the beginning of the test, which decreases until a plateau after about 10^3 cycles is reached. At complete fracture the dissipated energy evidently drops to zero. PBAT dissipates, under the same measurement conditions, less heat than PLA, but both polymers produce less energy dissipation than PBS as shown in Fig. 5(a).

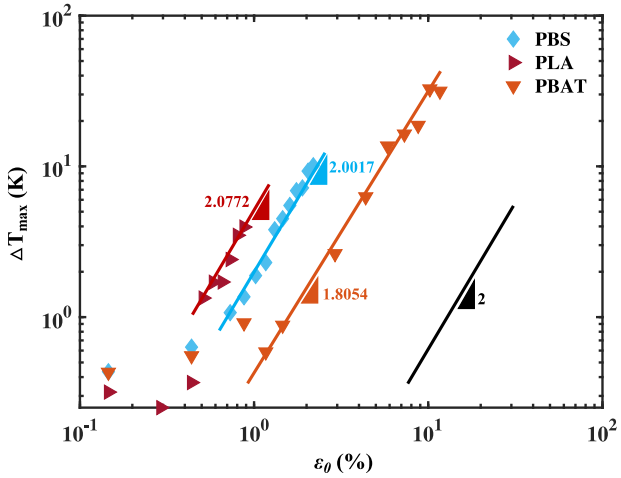

Fig. 7. Maximum temperature rise (ΔT_{max}) as a function of the strain amplitude for PBS, PBAT and PLA.

Fig. 5(b) shows that the loss factor (tan δ = E''/E') of PBS during fatigue has the highest value among the three polymers, leading to more energy dissipation in Fig. 5(a), because the loss modulus (E'') is correlated to energy dissipation via:

$$W_{diss} = \pi \varepsilon_0^2 E''(\varepsilon_0, t) \quad (5)$$

Here, the complex moduli ($|E^*|$) are extract by the ratio of stress amplitude (I_1) to the strain amplitude (ε_0), while the storage (E') and loss (E'') moduli can be obtained by multiplying I_1 by cosδ$_1$and sinδ$_1$, respectively. Although PBAT has higher tan δ than PLA (Fig. 5(b)), it releases less energy. This can be ascribed to its much lower complex moduli ($|E^*|$) as reported in Table 2. Consequently, a larger phase angle (δ) does not inherently result in higher loss modulus as $E'' = |E^*|$ sin δ (see Table 3).

4.3. Thermal stability in dynamic fatigue tests

Thermal analysis based on an increase of the surface temperature from the experimental observation under fatigue testing is an approach to estimate the fatigue limit of materials [55]. The temperature rise is strongly associated with the applied stress/strain amplitude under dynamic loading conditions [1,56].

Since the temperature rise for PLA under its maximum strain amplitude (~1%) is lower than for the other polymers tested and showing similar trends as for PBS, only the data of PBS and PBAT are

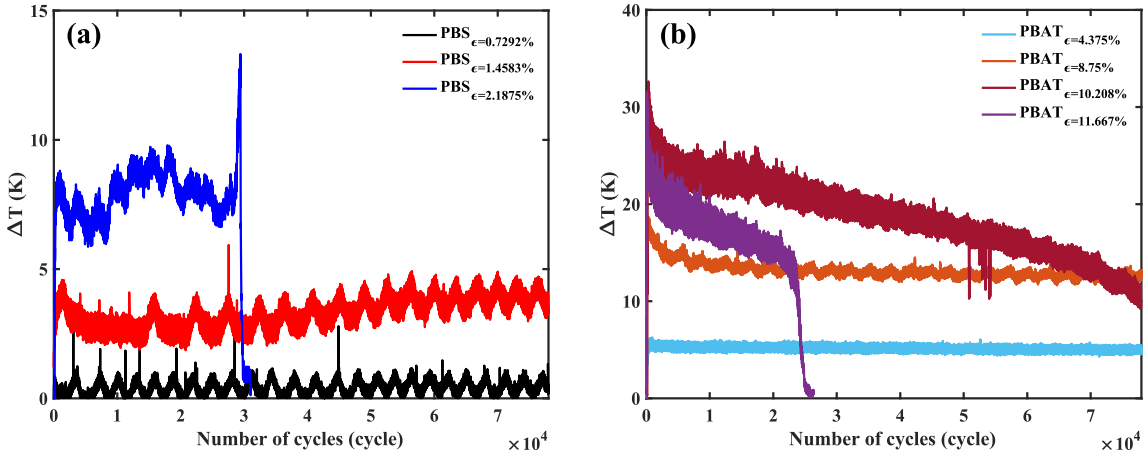

Fig. 6. Typical surface temperature evolution during fatigue tests at different strain amplitudes ($f = 5$ Hz) for: (a) PBS and (b) PBAT.

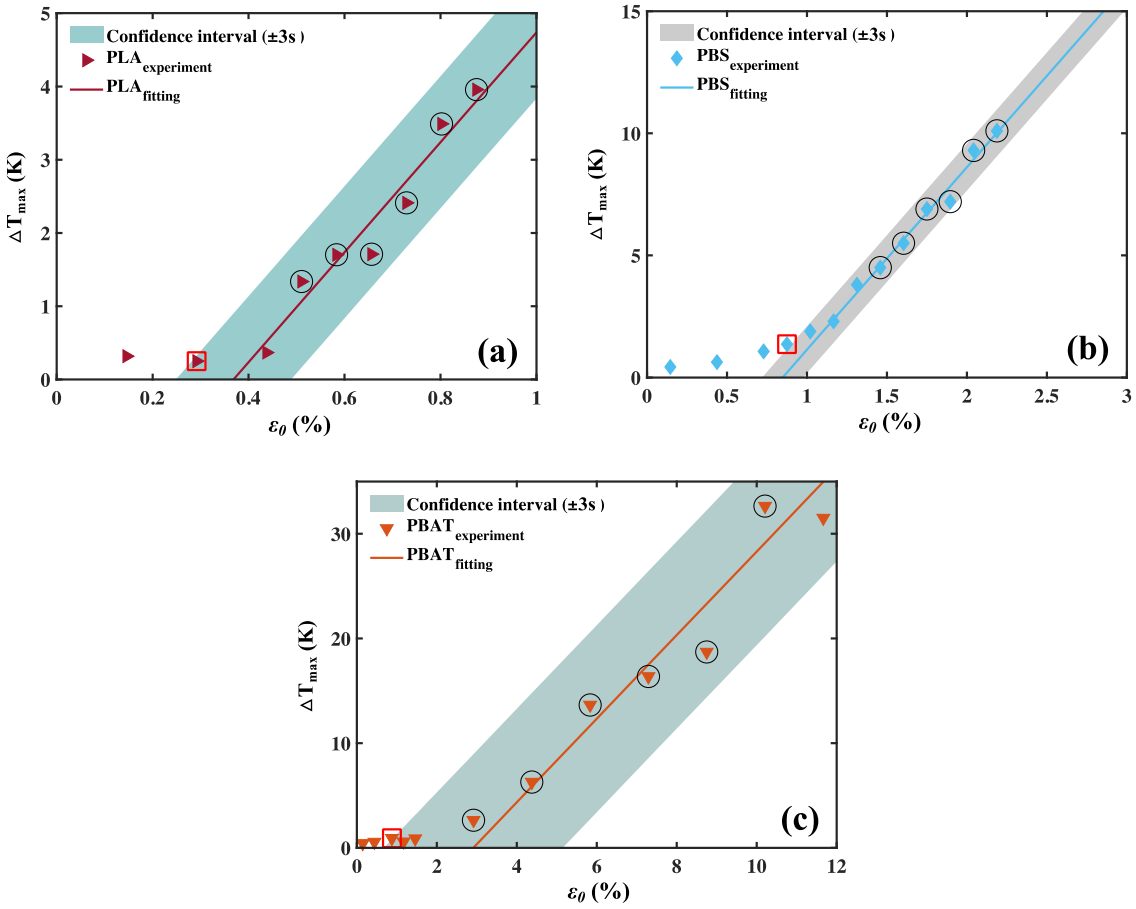

Fig. 8. Fatigue limit evaluation based on the maximum temperature rise for: (a) PLA, (b) PBS and (c) PBAT.

presented to show their different behaviors in terms of the mechanical-thermal coupling effect.

Fig. 6 reports the surface temperature rise (ΔT) monitored at different strain amplitude for PBS and PBAT. At the beginning of the test, the surface temperature of PBS rapidly increases and reaches a plateau. Increasing the strain amplitude considerably increases the temperature difference (ΔT). Similar trends can be observed for PBAT, except the temperature reaches a maximum value at first and then decreases monotonically instead of having a stationary value at high level of strain amplitude. The difference between PBS and PBAT at high strain amplitudes can be ascribed to the high susceptibility of PBAT to temperature changes associated with heat generation. Firstly, after crack initiation and propagation across the specimens, heat dissipation decreases due to lower mechanical property (E''). Secondly, PBAT has lower specific heat 0.2 W/(m·K) compared to PBS (2.25 W/(m·K)). This would lead to a 4–5 fold surface temperature decrease for PBAT compared to PBS under the same amount of energy generation. Therefore, both factors contribute to the different temperature behavior at high strain amplitudes between PBS and PBAT.

To better analyze the relationship between the maximum surface temperature rise (ΔT_{max}) and the applied strain amplitude (ε_0), Fig. 7 plots ΔT_{max} as a function of ε_0 for the investigated materials. A quadratic relation (Eq. (2)) between ΔT_{max} and ε_0 is observed above a critical strain amplitude depending on the material. However, no distinct trend can be concluded once the strain amplitude is below this critical strain. Therefore, this critical strain can be identified as a transition point to determine whether fatigue would happen at a given strain amplitude based on the surface temperature change. These information leads to the possibility of linking the surface temperature rise to the fatigue behavior since the applied strain amplitude can also highly affect the fatigue life as shown in Fig. 2. In our case, PLA has the highest temperature rise (ΔT_{max}) below $\varepsilon_0 = 0.875\%$ in Fig. 7 but dissipates much less energy than PBS as shown in Fig. 5. This is because the thermal conductivity of PLA (0.13 W/(m·K) [57]) is one order of magnitude less than PBS (2.25 W/(m·K) [58]). Another reason can be attributed to the fatigue process itself. For PBS it takes more cycles to reach the maximum temperature rise, as it occurs after the dissipated energy reached a plateau value as shown in Fig. 5.

According to Rosa et al. [56], a fingerprint of the surface temperature allows to rapidly determine the fatigue limit of materials. It actually gives an indication if the material has high fatigue resistance (10^6 cycles for example) below a critical stress/strain value. Their work also highlighted another important aspect: if the applied loading was below the fatigue limit of the material, the maximum temperature rise was limited. However, if the loading was above the fatigue limit, substantial temperature increase with distinct stages can be observed as shown in Fig. 6. These phenomena were closely related to the fatigue mechanisms as explained by Guo et al. [59]. Based on their theory, the relationship between self-heating and loading conditions originates from a change of heat generating mechanism during fatigue [60]. The main mechanism below the fatigue limit is viscoelastic dissipation, which only produces limited amount of heat per cycle. Once the loading conditions are above the fatigue limit, microplastic dissipation becomes the dominant heat generation source producing a large amount of heat per cycle. This difference can be used for fatigue limit assessment during thermal characterization. Fig. 7 shows a clear transition from lower to higher loads as the correlation between strain amplitude and maximum surface temperature rise in a log–log plot. For microplastic dissipation, self-heating as a function of strain amplitude can be fit to a linear relation on log–log scale with a slope of about 2 (1.81–2.08). If the material was

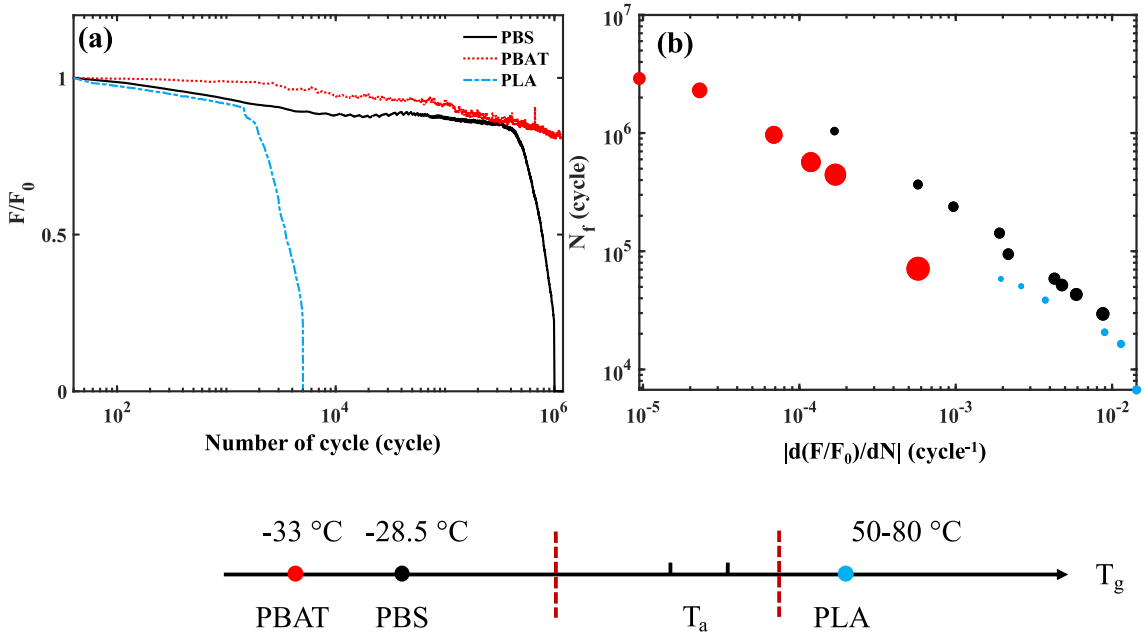

Fig. 9. (a) Evolution of the peak force degradation (F/F_0) as a function of the number of cycles (N) for fatigue tests at $\varepsilon_0 = 0.875\%$ and $f = 5$ Hz. (b) Correlation between the strain amplitude (ε_0), degradation rate ($d(F/F_0)/dN$) and fatigue life (N_f) for: PBS (•), PBAT (•) and PLA (•). The symbol size is proportional to the strain amplitudes (ε_0).

submitted to the identical heat generation mechanism (microplastic dissipation), the data should be within a statistical reproducibility range [56,59–61]. Otherwise, the data would deviate from the regression line due to a significant difference between the regimes of viscoelastic and microplastic dissipation. To assure a reliable and statistically significant analysis, the boundaries of $\pm 3\sigma$ were defined to include over 99% probability that microplastic dissipation points would fall into this interval as shown in Fig. 8. The standard deviation (s) was calculated from the distance (residues) of each point in the microplastic regime away from the regression line [62,63]. The data points scattered outside the intervals in Fig. 8 would be considered as viscoelastic dissipation.

Fig. 8 presents the evaluation of the fatigue limit for the investigated polymers. Six data points in the microplastic dissipation region, as marked by black circles, were selected as suggested by Guo et al.[59]

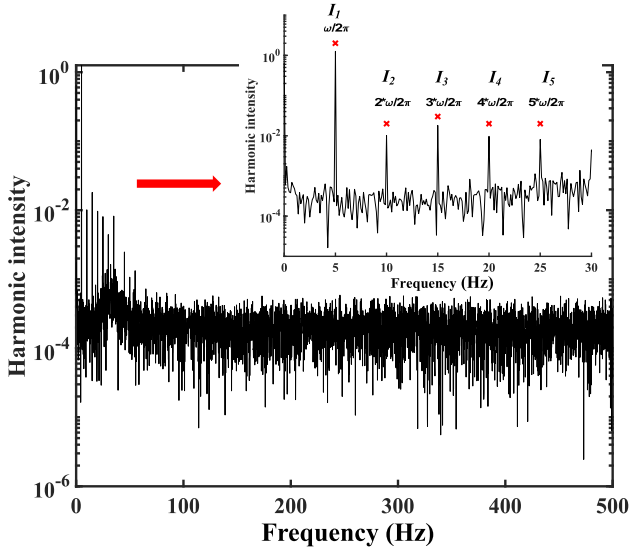

Fig. 10. Fourier spectra of the force response of PBS at $\varepsilon_0 = 0.875\%$ and $f = 5$ Hz. The inset shows the detailed harmonics at the beginning of the test.

and De Finis et al. [63] for the regression. Once the fit was established, the confidence interval can be outlined to classify the different regimes. Consequently, the fatigue limits of the materials can be defined as the first value outside the enclosed area from the left side. Our analysis indicates that the fatigue limit is 0.88% for PBS and PBAT, and 0.29% for PLA under the strain-controlled conditions tested ($f = 5$ Hz and $R = 0.13$). From Fig. 2, the fatigue life of PBS and PBAT both reached 10^6 cycles (criteria as the fatigue limit [1]) under the estimated fatigue limits, but it failed for PLA which had a fatigue lifetime of 10^4 cycles for a strain amplitude of 0.29%. Therefore, this method for a rapid determination of the fatigue limit seems to apply for PBS and PBAT, but overestimate the value for PLA. The main reason for this deviation might be the different behavior between ductile (PBAT and PBS) and brittle (PLA) materials (Fig. A.1). However, the conclusion that PBS and PBAT have longer fatigue life than PLA can still be made based on this analysis. Therefore, it can be of high interest for engineers to rapidly assess the suitability of each material for specific applications (comparative analysis).

4.4. Peak force degradation

Peak force degradation is one of the most commonly used parameters to analyze progressive damage during fatigue [64–66]. It represents the force degradation of the specimen allowing to identify the fatigue criterion in terms of number of cycles (N) necessary to reduce a damage index [65]. The evolution of the maximum load (F) for each cycle normalized by the value of the first cycle (F_0) is presented as a function of the number of cycles (N) in Fig. 9a. It can be seen, that the loss of load (F/F_0) is slow at first, followed by an abrupt decrease once crack onset occurs. However, the degradation rate among the three biodegradable polymers can be clearly distinguished in the early stage in the order of PLA > PBS > PBAT. To further investigate the correlation between strain amplitude, loading degradation and fatigue life, Fig. 9b plots the degradation rate ($d(F/F_0)/dN$) as a function of the fatigue life (N_f). In Fig. 9b the symbol size represents the values of the strain amplitude (ε_0). It can be seen that larger absolute value of degradation rate ($|\, d(F/F_0)/dN\,|$) resulted in shorter fatigue life for all materials. This is as expected, since the strain amplitude directly determines the degradation rate as

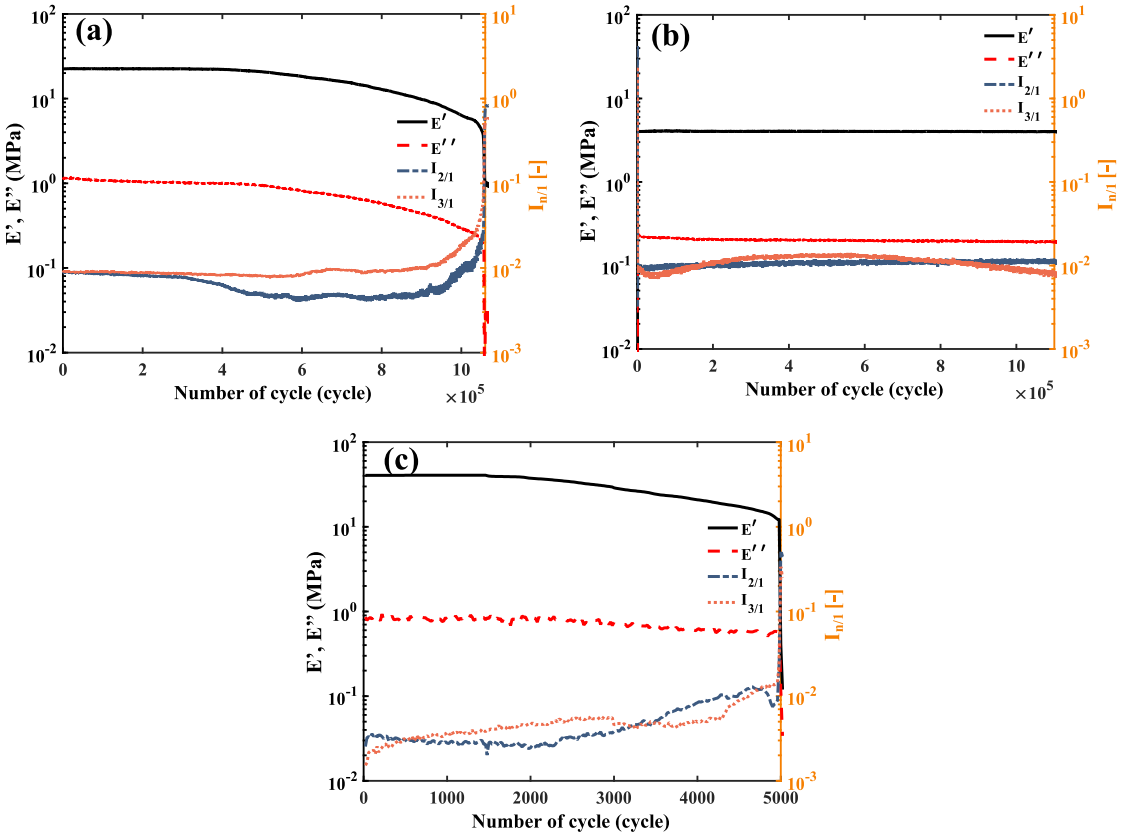

Fig. 11. Storage modulus (E'), loss modulus (E'') and nonlinear parameters ($I_{2/1}$, $I_{3/1}$) as a function of the cycle number for: (a) PBS, (b) PBAT and (c) PLA (ε_0 = 0.875% and f = 5 Hz).

shown in Fig. 9b. However, even with much larger strain amplitudes, PBAT cannot degrade as fast as PLA. For example, the degradation rate of PBAT for a strain amplitude ε_0 = 11.7% reaches $|\, d(F/F_0)/dN \,|$ = 0.0005/cycle, while PLA had an absolute degradation rate of 0.002/cycle when submitted to only ε_0 = 0.15%. This significant difference can be attributed to the different glass transition temperature (T_g) of the materials. The T_g of PLA ranges from 50 to 80 °C, but PBAT has much lower T_g = –33 °C. Therefore, under the testing conditions (T_a = 23 °C), PLA becomes brittle, but PBAT was ductile, which can also be confirmed by the moduli in Table 2. Therefore, the crack is initiated after the same cycle number at lower deformation for brittle PLA compared to ductile PBS and PBAT. Such difference further leads to fast crack propagation for PLA showing higher degradation rate. Also, PBS shows a similar trend regarding loading loss, but the performance is intermediate among the three polymers investigated.

4.5. Nonlinear analysis of fatigue tests

Fig. 10 shows the typical Fourier spectra of the stress response for PBS at ε_0 = 0.875% and f = 5 Hz as an example. The fundamental harmonic ($I(\omega_1)$) and peaks for higher harmonics, such as $I(2\omega_1)$, $I(3\omega_1)$, $I(4\omega_1)$ and $I(5\omega_1)$, are shown in the inset which are associated with the nonlinear behavior of the material. Also, the peaks for higher frequencies ($n > 10$) are considered as within the noise level (less than 10^{-3}). Therefore, the values are considered significant to analyze up to the third higher harmonics ($I_{2/1}$ and $I_{3/1}$) as they can provide the most essential information to capture the nonlinear features [43].

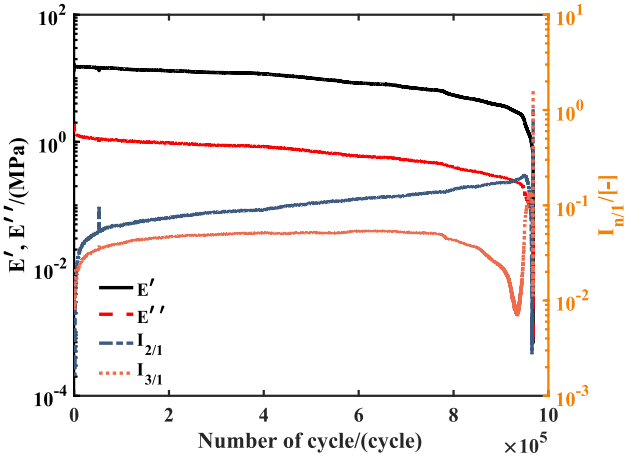

Fig. 12. Storage modulus (E'), loss modulus (E'') and nonlinear parameters ($I_{2/1}$, $I_{3/1}$) as a function of the cycle number for PBAT (ε_0 = 5.83% and f = 5 Hz).

Fig. 11 compares the linear parameters, such as E' and E'', as well as the nonlinear parameters, such as $I_{2/1}$ and $I_{3/1}$, for PBS, PBAT and PLA under the same testing conditions (ε_0 = 0.875% and f = 5 Hz). Both E' and E'' decrease with ongoing fatigue for PBS and PLA, but remain almost constant for PBAT, as the strain amplitude is not high enough to significantly damage the specimen and to break it. In more details, the

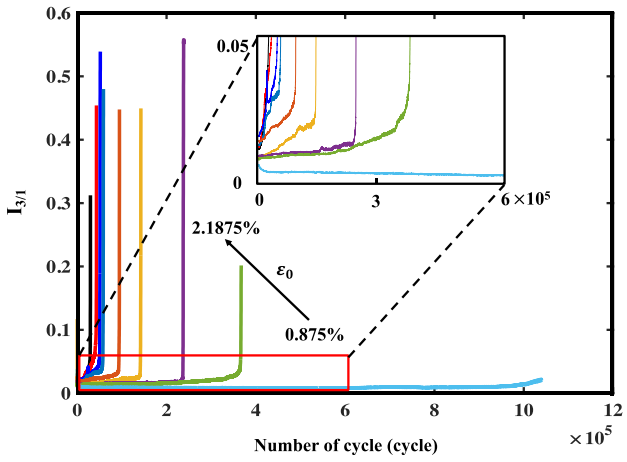

Fig. 13. Evolution of $I_{3/1}$ as a function of the number of cycles (N) for PBS at different strain amplitudes (ε_0 = 0.875–2.1875%) and f = 5 Hz.

linear parameters (E') of PBS and PLA stay constant until crack onset. Afterwards, the value decreases with increasing number of cycles, until a sharp decrease occurs due to complete fracture. However, the slope ($|dE'/dN|$) for PLA is much steeper. As proposed by Hirschberg et al. [4], the rate of change of the complex modulus can be correlated to crack propagation. Thus, it indicates that the crack growth in PLA is faster than PBS. Similarly, the loss modulus (E'') of PLA decreases much faster than PBS. Since PBAT does not generate a crack before 10^6 cycles for the conditions tested (ε_0 = 0.875% and f = 5 Hz), no variation of the linear parameters is observed. However, the absolute value of E' and E'' show similar trend as PBS at larger strain amplitude (Fig. 12).

The intensity of the nonlinear parameters ($I_{2/1}$ and $I_{3/1}$) at the beginning for PLA is lower than for PBS and PBAT, but gradually increase until the specimen completely breaks. Before crack initiation, $I_{3/1}$ slightly changes for PBS and PBAT. Once a crack started, similar to PBS, $I_{3/1}$ grows at a constant rate ($dI_{3/1}/dN$) during crack propagation. However, no general trend can be concluded from the $I_{2/1}$ evolution before complete fracture. Ultimately, the intensities of $I_{2/1}$ and $I_{3/1}$ sharply increase when the specimen breaks. Although the nonlinear parameters barely change for PBAT during the test at ε_0 = 0.875% (Fig. 11), the intensity of $I_{2/1}$ becomes more dominant than $I_{3/1}$ at larger strain amplitudes (ε_0 = 5.83%) as shown in Fig. 12 and increases with the number of cycles. Under sufficiently large amplitude oscillatory deformations, the nonlinearity of PBAT becomes noticeable, especially for even harmonics ($I_{2/1}$), and the presence of even harmonics in the stress response is the result of asymmetry in the material [67,68].

To characterize the nonlinear behavior of PBS, $I_{3/1}$ is used due to its stronger intensity and clearer trend. As shown in Fig. 13, the evolution of $I_{3/1}$ at different strain amplitudes reveals the trends correlating with the strain amplitude. The intensity of $I_{3/1}$ increases with increasing amplitude. In the inset of Fig. 13, $I_{3/1}(N)$ is shown in detail. With increasing strain amplitude, the intensity of $I_{3/1}(N)$ increases faster as a function of the cycle number, while the fatigue life (N_f) decreases. Therefore, a correlation for $dI_{3/1}/dN$ based on $I_{3/1}$ with fatigue life (N_f) can also be made for PBS. Using the rate of change of $I_{3/1}$ ($dI_{3/1}/dN$) as an indicator of polymer fatigue was proposed by Hirschberg et al. [5,39,43].

The evolution of the nonlinear parameters of PBAT is different from PBS, as the even higher harmonic ($I_{2/1}$) becomes dominant and informative. Fig. 14 shows a transition point in the $I_{2/1}$ curve during fatigue which is shifting to larger number of cycles. The intensity decreases when PBAT is submitted to smaller strain amplitudes. The presence of higher harmonics, such as $I_{2/1}$, implies an asymmetric stress response. Another possible reason for the transition point is the asymmetric stress response itself and buckling overlap, thus cancelling each other as their phase angles are shifted by π [42]. To quantify this phenomenon, a mathematical description based on a modified Kelvin-Voigt model was proposed as [42]:

$$\sigma = E\varepsilon_0 sin\omega_1 t + E\varepsilon_s + \eta_0 + \sum_{n=1}^{\infty}\eta_n(\omega_1\varepsilon_0 cos\omega_1 t)^n - \frac{|\chi|+\chi}{2|\chi|}[B_1 sin\omega_1 t + \sum_{n=2,4,6,\cdots}^{\infty} B_n(\omega_1\varepsilon_0 cos\omega_1 t)^n]\# \quad (6)$$

and its *Fourier* transform can be written as:

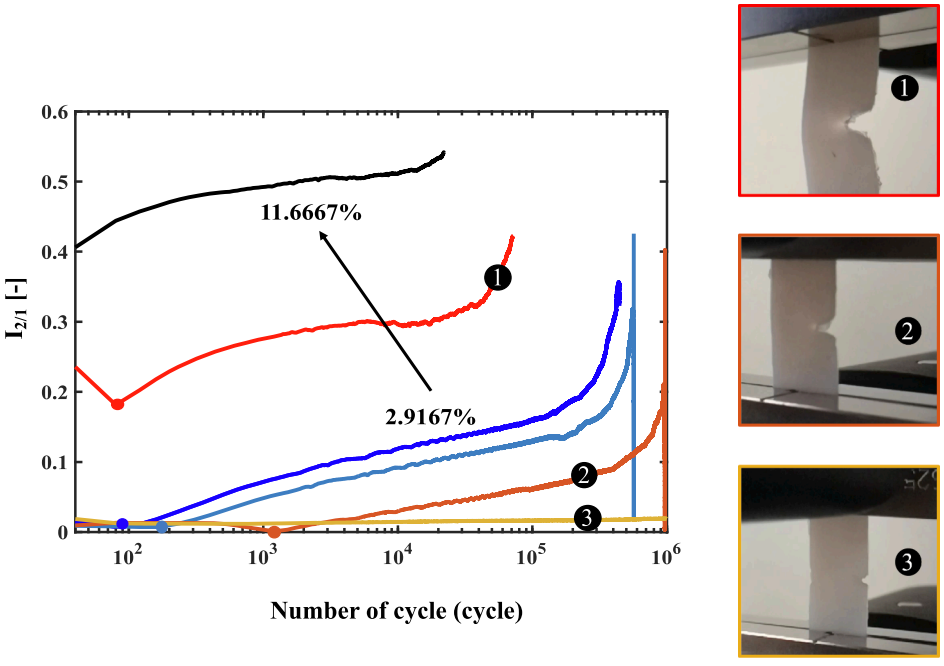

Fig. 14. Evolution of $I_{2/1}$ as a function of the number of cycles (N) for PBAT at different strain amplitudes, ε_0 = 2.92%, 5.83%, 7.29%, 8.75%, 10.94% and 11.67% at f = 5 Hz.

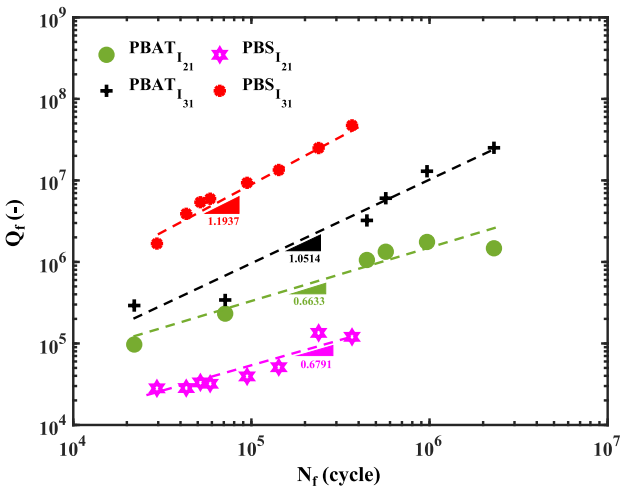

Fig. 15. Cumulative nonlinearity (Q_f) based on $I_{2/1}$ and $I_{3/1}$ as a function of the number of cycles to failure (N_f) under fatigue for PBS and PBAT.

$$\sigma = I_0 + \underbrace{A_1 sin(\omega_1 t + \delta_1) - \frac{|\chi| + \chi}{2|\chi|} B_1 sin\omega_1 t}_{I_1 sin(\omega_1 t + \delta_1)} + \underbrace{\sum_{n=2}^{\infty} A_n cosn\omega_1 t - \frac{|\chi| + \chi}{2|\chi|} \sum_{n=2,4,6,\ldots}^{\infty} B_n cos\ n\omega_1 t}_{\sum_{n=2}^{\infty} I_n cosn\omega_1 t} \quad (7)$$

In this model, if the specimen is stretched beyond a critical deformation, plastic deformation occurs. Buckling starts when the applied force (F) at the minimum strain value exceeds the critical value for buckling (F_{bc}) as:

$$\chi = F - F_{bc} > 0\# \quad (8)$$

This leads to even harmonics being different on the right-hand side in the *4th* and *5th* terms of Eq. (7) when n is even leading to lower even harmonics ($I_{2/1}$) before buckling occurs. Therefore, $I_{2/1}$ is a very interesting indicator to predict buckling. However, there is no significant buckling observed during PBAT testing in our cases (low strain amplitudes). To confirm this, imaging was performed for selected tests with comparatively large (10.9%), intermediate (5.83%) and small (2.92%) strain amplitude as shown in Fig. 14. Obviously, buckling is observed at large strain amplitude, but it is difficult to see at intermediate and small strain amplitudes. Using frame-by-frame analysis, buckling for intermediate strain amplitude is observed in picture #2 in Fig. 14, but not for the small strain amplitude (picture #3). This corresponds to the minima of $I_{2/1}$ for large to intermediate strain amplitudes, but not for the small one.

Fig. 15 presents the cumulative nonlinearity parameter (Q_f) as a function of the fatigue lifetime (N_f) to compare the fatigue behavior of PBS and PBAT as typical examples since they have similar fatigue lifetime range under the conditions tested. The fatigue life follows a power-law relation with respect to ${}^nQ_f$ as:

$${}^nQ_f = {}^nA_Q\ N_f^{k_n} \quad (9)$$

It is found that the exponents k_3 (k_2) in terms of ${}^3Q_f$ (${}^2Q_f$) vs. N_f have different values for the different materials, PBS = 1.19 (0.68) and PBAT = 1.05 (0.66). The exponent k_3 is very close to 1 for PBAT which indicates small ${}^3Q$ change for different strain amplitudes. Symmetric nonlinearity (${}^3Q_f$) is more intensive for PBS than PBAT. The exponents of ${}^2Q_f$ are close to each other for PBS ($k_2 = 0.663$) and PBAT ($k_2 = 0.679$). This difference between ${}^2Q_f$ and ${}^3Q_f$ of PBS and PBAT must come from the material itself since the imposed cyclic loading is completely symmetric. It also indicates that ${}^2Q_f$ correlated to the fatigue lifetime for both PBS and PBAT instead of summing up noise and possibly being a good indicator to relate to the cumulative nonlinearity vs. fatigue. For both materials, ${}^nQ_f$ increases with increasing fatigue lifetime. This analysis should now be applied to other materials to determine its suitability as a more universal criterion.

5. Conclusion

Mechanical fatigue tests in strain-controlled tension–tension are performed for notched specimens of PLA, PBS and PBAT. The stress response is analyzed to characterize the fatigue behaviors of these biodegradable polymers. The evolution of surface temperature is used to understand the thermomechanical coupling effect during materials' fatigue. The nonlinear contribution of the materials is investigated by Fourier transform decomposition. Therefore, several conclusions can be drawn based on the obtained experimental results.

The ductile PBS and PBAT had competitive fatigue lifetime up to 10^6 cycles compared to brittle PLA which is two decades less. During the cyclic test, the out-of-phase behavior between imposed strain and response stress is appreciable for PBS but marginal for PLA and PBAT. Therefore, larger energy dissipation is expected for PBS as well. Under the condition of $\varepsilon_0 = 0.875\%$ and $f = 5$ Hz, PBS can generate almost 10-fold heat dissipation over PBAT and PLA at the beginning of the tests. With ongoing cyclic loadings, force degradation is observed for all three materials, but PLA had the highest absolute rate of 0.002/cycle, which is at least 4 times faster than PBAT. Further investigations revealed that the degradation rate depends on the strain amplitude. Surface temperature increased with strain amplitudes for all polymers and a quadratic relation between ΔT_{max} and ε_0 can be approximated. Even ($I_{2/1}$) and odd ($I_{3/1}$) harmonics in the stress can be well detected to characterize nonlinearity during fatigue tests under a range of conditions. It was found that $I_{2/1}$ is sensitive to predict buckling initiation for PBAT and $I_{3/1}$ is highly fatigue sensitive for PBS. The cumulative nonlinearity parameter ${}^3Q_f$ was shown to be a strong criterion to rationalize the fatigue behavior of PBS and ${}^2Q_f$ can be used as a fatigue indicator for both PBS and PBAT.

Declaration of Competing Interest

The authors declare that they have no known competing financial interests or personal relationships that could have appeared to influence the work reported in this paper.

Acknowledgement

The authors acknowledge the financial support of the Natural Science and Engineering Research Council of Canada (NSERC).

Appendix

See Fig. A1.

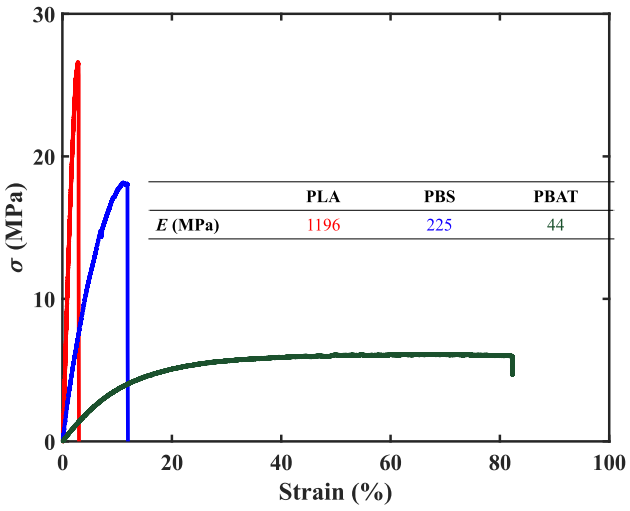

Fig. A1. Stress–strain curves of PLA, PBS and PBAT. The tests were performed at a rate of 5 mm/min and room temperature.

References

[1] Hirschberg V, Wilhelm M, Rodrigue D. Combining mechanical and thermal surface fourier transform analysis to follow the dynamic fatigue behavior of polymers. Polym Test 2021;96:107070. https://doi.org/10.1016/j.polymertesting.2021.107070.

[2] Hirschberg V, Schwab L, Cziep M, Wilhelm M, Rodrigue D. Influence of molecular properties on the mechanical fatigue of polystyrene (PS) analyzed via Wöhler curves and Fourier Transform rheology. Polymer 2018;138:1–7. https://doi.org/10.1016/j.polymer.2018.01.042.

[3] Hirschberg V, Wilhelm M, Rodrigue D. Cumulative nonlinearity as a parameter to quantify mechanical fatigue. Fatigue Fract Eng Mater Struct 2020;43(2):265–76. https://doi.org/10.1111/ffe.13120.

[4] Hirschberg V, Faust L, Wilhelm M, Rodrigue D. Universal strain-life curve exponents for thermoplastics and elastomers under tension-tension and torsion. Macromol Mater Eng 2021;306(8):2100165. https://doi.org/10.1002/mame.202100165.

[5] Hirschberg V, Lacroix F, Wilhelm M, Rodrigue D. Fatigue analysis of brittle polymers via Fourier transform of the stress. Mech Mater 2019;137:103100. https://doi.org/10.1016/j.mechmat.2019.103100.

[6] Lamnii H, Nait Abdelaziz M, Ayoub G, Colin X, Maschke U. Experimental investigation and modeling attempt on the effects of ultraviolet aging on the fatigue behavior of an LDPE semi-crystalline polymer. Int J Fatigue 2021;142:105952. https://doi.org/10.1016/j.ijfatigue.2020.105952.

[7] United Nations. Adoption of the Paris agreement; 2015. <https://unfccc.int/resource/docs/2015/cop21/eng/l09r01.pdf> [accessed 15 November 2021].

[8] Zheng J, Suh S. Strategies to reduce the global carbon footprint of plastics. Nat Clim Change 2019;9(5):374–8. https://doi.org/10.1038/s41558-019-0459-z.

[9] Environment and Climate Change Canada. Economic study of the Canadian plastic industry, markets and waste; 2019. <https://publications.gc.ca/collections/collection_2019/eccc/En4-366-1-2019-eng.pdf> [accessed 15 November 2021].

[10] Walker TR, McGuinty E, Charlebois S, Music J. Single-use plastic packaging in the Canadian food industry: consumer behavior and perceptions. Sci Commun 2021;8:1–1. doi: 10.1057/s41599-021-00747-4.

[11] Li J, He Y, Inoue Y. Thermal and mechanical properties of biodegradable blends of poly(L-lactic acid) and lignin. Polym Int 2003;52(6):949–55. https://doi.org/10.1002/pi.1137.

[12] Kargarzadeh H, Huang J, Lin N, Ahmad I, Mariano M, Dufresne A, et al. Recent developments in nanocellulose-based biodegradable polymers, thermoplastic polymers, and porous nanocomposites. Prog Polym Sci 2018;87:197–227. https://doi.org/10.1016/j.progpolymsci.2018.07.008.

[13] Wu C, Zhang X, Wang X, Gao Q, Li X. Surface modification of cellulose nanocrystal using succinic anhydride and its effects on poly(butylene succinate) based composites. Cellulose 2019;26(5):3167–81. https://doi.org/10.1007/s10570-019-02292-5.

[14] Ohkita T, Lee S-H. Crystallization behavior of poly(butylene succinate)/corn starch biodegradable composite. J Appl Polym Sci 2005;97(3):1107–14. https://doi.org/10.1002/app.21741.

[15] Bao Le, Chen Y, Zhou W, Wu Y, Huang Y. Bamboo fibers @ poly(ethylene glycol)-reinforced poly(butylene succinate) biocomposites. J Appl Polym Sci 2011;122(4):2456–66. https://doi.org/10.1002/app.34365.

[16] Liu L, Yu J, Cheng L, Yang X. Biodegradability of poly(butylene succinate) (PBS) composite reinforced with jute fibre. Polym Degrad Stabil 2009;94(1):90–4. https://doi.org/10.1016/j.polymdegradstab.2008.10.013.

[17] Bin T, Qu J-P, Liu L-M, Feng Y-H, Hu S-x, Yin X-C. Non-isothermal crystallization kinetics and dynamic mechanical thermal properties of poly(butylene succinate) composites reinforced with cotton stalk bast fibers. Thermochim Acta 2011;525(1-2):141–9. https://doi.org/10.1016/j.tca.2011.08.003.

[18] Nam TH, Ogihara S, Tung NH, Kobayashi S. Effect of alkali treatment on interfacial and mechanical properties of coir fiber reinforced poly(butylene succinate) biodegradable composites. Compos B Eng 2011;42(6):1648–56.

[19] Thirmizir MZA, Ishak ZAM, Taib RM, Rahim S, Jani SM. Kenaf-bast-fiber-filled biodegradable poly(butylene succinate) composites: Effects of fiber loading, fiber length, and maleated poly(butylene succinate) on the flexural and impact properties. J Appl Polym Sci 2011;122(5):3055–63. https://doi.org/10.1002/app.34046.

[20] Joy J, Jose C, Varanasi SB, Mathew P. L, Thomas S, Pilla S. Preparation and characterization of poly(butylene succinate) bionanocomposites reinforced with cellulose nanofiber extracted from helicteres isora plant. J Renew Mater 2016;4(5):351–64. https://doi.org/10.7569/JRM.2016.634128.

[21] Kim H-S, Yang H-S, Kim H-J. Biodegradability and mechanical properties of agro-flour-filled polybutylene succinate biocomposites. J Appl Polym Sci 2005;97(4):1513–21. https://doi.org/10.1002/app.21905.

[22] Flores ED, Funabashi M, Kunioka M. Mechanical properties and biomass carbon ratios of poly(butylene succinate) composites filled with starch and cellulose filler using furfural as plasticizer. J Appl Polym Sci 2009;112(6):3410–7. https://doi.org/10.1002/app.29777.

[23] Sahoo S, Misra M, Mohanty AK. Enhanced properties of lignin-based biodegradable polymer composites using injection moulding process. Compos Part A Appl Sci Manuf 2011;42(11):1710–8.

[24] Ferreira FV, Cividanes LS, Gouveia RF, Lona LMF. An overview on properties and applications of poly(butylene adipate- *co* -terephthalate)-PBAT based composites. Polym Eng Sci 2019;59(s2):E7–15. https://doi.org/10.1002/pen.24770.

[25] Dammak M, Fourati Y, Tarrés Q, Delgado-Aguilar M, Mutjé P, Boufi S. Blends of PBAT with plasticized starch for packaging applications: Mechanical properties, rheological behaviour and biodegradability. Ind Crops Prod 2020;144:112061. https://doi.org/10.1016/j.indcrop.2019.112061.

[26] Morelli CL, Belgacem MN, Branciforti MC, Bretas RES, Crisci A, Bras J. Supramolecular aromatic interactions to enhance biodegradable film properties through incorporation of functionalized cellulose nanocrystals. Compos Part A Appl Sci Manuf 2016;83:80–8. https://doi.org/10.1016/j.compositesa.2015.10.038.

[27] Pinheiro IF, Ferreira FV, Souza DHS, Gouveia RF, Lona LMF, Morales AR, et al. Mechanical, rheological and degradation properties of PBAT nanocomposites reinforced by functionalized cellulose nanocrystals. Eur Polym J 2017;97:356–65. https://doi.org/10.1016/j.eurpolymj.2017.10.026.

[28] Zhang X, Ma P, Zhang Y. Structure and properties of surface-acetylated cellulose nanocrystal/poly(butylene adipate-co-terephthalate) composites. Polym Bull 2016;73(7):2073–85. https://doi.org/10.1007/s00289-015-1594-y.

[29] Mukherjee T, Czaka M, Kao N, Gupta RK, Choi J, Bhattacharya S. Dispersion study of nanofibrillated cellulose based poly(butylene adipate-co-terephthalate) composites. Carbohydr Polym 2014;102:537–42. https://doi.org/10.1016/j.carbpol.2013.11.047.

[30] Chen JH, Yang MC. Preparation and characterization of nanocomposite of maleated poly(butylene adipate-co-terephthalate) with organoclay. Mater Sci Eng C 2015;46:301–8. https://doi.org/10.1016/j.msec.2014.10.045.

[31] Lin N, Huang J, Chang PR, Feng J, Yu J. Surface acetylation of cellulose nanocrystal and its reinforcing function in poly(lactic acid). Carbohydr Polym 2011;83(4):1834–42. https://doi.org/10.1016/j.carbpol.2010.10.047.

[32] Rhim J-W, Hong S-I, Ha C-S. Tensile, water vapor barrier and antimicrobial properties of PLA/nanoclay composite films. LWT – Food Sci Technol 2009;42(2):612–7. https://doi.org/10.1016/j.lwt.2008.02.015.

[33] Armentano I, Bitinis N, Fortunati E, Mattioli S, Rescignano N, Verdejo R, et al. Multifunctional nanostructured PLA materials for packaging and tissue engineering. Prog Polym Sci 2013;38(10–11):1720–47. https://doi.org/10.1016/j.progpolymsci.2013.05.010.

[34] Afrose MF, Masood SH, Iovenitti P, Nikzad M, Sbarski I. Effects of part build orientations on fatigue behaviour of FDM-processed PLA material. Prog Addit Manuf 2016;1(1–2):21–8. https://doi.org/10.1007/s40964-015-0002-3.

[35] Ezeh OH, Susmel L. Fatigue strength of additively manufactured polylactide (PLA): effect of raster angle and non-zero mean stresses. Int J Fatigue 2019;126:319–26. https://doi.org/10.1016/j.ijfatigue.2019.05.014.

[36] Ezeh OH, Susmel L. On the notch fatigue strength of additively manufactured polylactide (PLA). Int J Fatigue 2020;136:105583. https://doi.org/10.1016/j.ijfatigue.2020.105583.

[37] Cicero S, Martínez-Mata V, Castanon-Jano L, Alonso-Estebanez A, Arroyo B. Analysis of notch effect in the fracture behaviour of additively manufactured PLA and graphene reinforced PLA. Theor Appl Fract Mech 2021;114:103032. https://doi.org/10.1016/j.tafmec.2021.103032.

[38] Vanaei HR, Shirinbayan M, Vanaei S, Fitoussi J, Khelladi S, Tcharkhtchi A. Multi-scale damage analysis and fatigue behavior of PLA manufactured by fused deposition modeling (FDM). Rapid Prototyp J 2021;27(2):371–8. https://doi.org/10.1108/RPJ-11-2019-0300.

[39] Hirschberg V, Wilhelm M, Rodrigue D. Fatigue life prediction via the time-dependent evolution of linear and nonlinear mechanical parameters determined via Fourier transform of the stress. J Appl Polym Sci 2018;135(33):46634. https://doi.org/10.1002/app.46634.

[40] Hyun K, Wilhelm M, Klein CO, Cho KS, Nam JG, Ahn KH, et al. A review of nonlinear oscillatory shear tests: Analysis and application of large amplitude oscillatory shear (LAOS). Prog Polym Sci 2011;36(12):1697–753. https://doi.org/10.1016/j.progpolymsci.2011.02.002.

[41] Wilhelm M. Fourier-transform rheology. Macromol Mater Eng 2002;287:83–105. https://doi.org/10.1002/1439-2054(20020201)287:2<83::AID-MAME83>3.0.CO;2-B.
[42] Hirschberg V, Wilhelm M, Rodrigue D. Fourier transform fatigue analysis of the stress in tension/tension of HDPE and PA6. Polym Eng Sci 2021;61(4):993–1006. https://doi.org/10.1002/pen.25616.
[43] Hirschberg V, Wilhelm M, Rodrigue D. Fatigue behavior of polystyrene (PS) analyzed from the Fourier transform (FT) of stress response: first evidence of I2/1(N) and I3/1(N) as new fingerprints. Polym Test 2017;60:343–50. https://doi.org/10.1016/j.polymertesting.2017.04.001.
[44] Hyun K, Baik ES, Ahn KH, Lee SJ, Sugimoto M, Koyama K. Fourier-transform rheology under medium amplitude oscillatory shear for linear and branched polymer melts. J Rheol 2007;51(6):1319–42. https://doi.org/10.1122/1.2790072.
[45] Hyun K, Wilhelm M. Establishing a new mechanical nonlinear coefficient Q from FT-rheology: first investigation of entangled linear and comb polymer model systems. Macromolecules 2009;42(1):411–22. https://doi.org/10.1021/ma8017266.
[46] Cziep MA, Abbasi M, Heck M, Arens L, Wilhelm M. Effect of molecular weight, polydispersity, and monomer of linear homopolymer melts on the intrinsic mechanical nonlinearity $^3Q_0(\omega)$ in MAOS. Macromolecules 2016;49(9):3566–79. https://doi.org/10.1021/acs.macromol.5b0270610.1021/acs.macromol.5b02706.s001.
[47] Xu J, Guo B-H. Poly(butylene succinate) and its copolymers: Research, development and industrialization. Biotechnol J 2010;5(11):1149–63. https://doi.org/10.1002/biot.201000136.
[48] Lannace S, Sorrentino L, Di Maio E. Biodegradable biomedical foam scaffolds. In: Netti Paolo A, editor. Biomedical foams for tissue engineering applications. Oxford: Woodhead Publishing; 2014. p. 163–87. https://doi.org/10.1533/9780857097033.1.163.
[49] Mecking S. Nature or Petrochemistry?—Biologically degradable materials. Angew Chem Int Ed 2004;43(9):1078–85. https://doi.org/10.1002/anie.200301655.
[50] Rudnik E. Compostable polymer properties and packaging applications. In: Ebnesajjad S, editor. Plastic films in food packaging: materials, technology and applications. Oxford: Elsevier; 2013. p. 217–48. https://doi.org/10.1016/B978-1-4557-3112-1.00013-2.
[51] Fujimaki T. Processability and properties of aliphatic polyesters, 'BIONOLLE', synthesized by polycondensation reaction. Polym Degrad Stab 1998;59(1–3):209–14. https://doi.org/10.1016/S0141-3910(97)00220-6.
[52] Yokohara T, Yamaguchi M. Structure and properties for biomass-based polyester blends of PLA and PBS. Eur Polym J 2008;44(3):677–85. https://doi.org/10.1016/j.eurpolymj.2008.01.008.
[53] Supthanyakul R, Kaabbuathong N, Chirachanchai S. Poly(L-lactide-b-butylene succinate-b-L-lactide) triblock copolymer: a multi-functional additive for PLA/PBS blend with a key performance on film clarity. Polym Degrad Stab 2017;142:160–8. https://doi.org/10.1016/j.polymdegradstab.2017.05.029.
[54] Fang M, Zhu Y, Hjalmarsson H. On anti-aliasing filtering and over-sampling scheme in system identification. Comput Chem Eng 2017;106:572–81. https://doi.org/10.1016/j.compchemeng.2017.07.010.
[55] Meneghetti G. Analysis of the fatigue strength of a stainless steel based on the energy dissipation. Int J Fatigue 2007;29(1):81–94. https://doi.org/10.1016/j.ijfatigue.2006.02.043.
[56] La Rosa G, Risitano A. Thermographic methodology for rapid determination of the fatigue limit of materials and mechanical components. Int J Fatigue 2000;22:65–73. https://doi.org/10.1016/S0142-1123(99)00088-2.
[57] Lebedev SM, Gefle OS, Amitov ET, Berchuk DY, Zhuravlev DV. Poly(lactic acid)-based polymer composites with high electric and thermal conductivity and their characterization. Polym Test 2017;58:241–8. https://doi.org/10.1016/j.polymertesting.2016.12.033.
[58] Wei L, Chen JF, He QY, Teng W. Study of lattice thermal conductivity of PbS. J Alloys Compd 2014;584:381–4. https://doi.org/10.1016/j.jallcom.2013.09.081.
[59] Guo S, Liu X, Zhang H, Yan Z, Fang H. Fatigue performance evaluation of AZ31B magnesium alloy based on statistical analysis of self-heating. Materials 2021;14:2251. https://doi.org/10.3390/ma14092251.
[60] Guo Q, Guo X, Fan J, Syed R, Wu C. An energy method for rapid evaluation of high-cycle fatigue parameters based on intrinsic dissipation. Int J Fatigue 2015;80:136–44. https://doi.org/10.1016/j.ijfatigue.2015.04.016.
[61] Fargione G, Geraci A, La Rosa G, Risitano A. Rapid determination of the fatigue curve by the thermographic method. Int J Fatigue 2002;24:11–9. https://doi.org/10.1016/S0142-1123(01)00107-4.
[62] Pugachev VS. Probability theory and mathematical statistics for engineers. 1st ed. London: CRC Press; 2014. Doi: 10.1201/9781482267761.
[63] De Finis R, Palumbo D, Ancona F, Galietti U. Fatigue limit evaluation of various martensitic stainless steels with new robust thermographic data analysis. Int J Fatigue 2015;74:88–96. https://doi.org/10.1016/j.ijfatigue.2014.12.010.
[64] Bezazi AR, El Mahi A, Berthelot JM, Bezzazi B. Flexural fatigue behavior of cross-ply laminates: an experimental approach. Strength Mater 2003;35:149–61. https://doi.org/10.1023/A:1023762528362.
[65] Berthelot JM. Relation between amplitudes and rupture mechanisms in composite materials. J Reinf Plast Compos 1988;7(3):284–99. https://doi.org/10.1177/073168448800700306.
[66] Bezazi A, Scarpa F. Tensile fatigue of conventional and negative Poisson's ratio open cell PU foams. Int J Fatigue 2009;31(3):488–94. https://doi.org/10.1016/j.ijfatigue.2008.05.005.
[67] Dötsch T, Pollard M, Wilhelm M. Kinetics of isothermal crystallization in isotactic polypropylene monitored with rheology and Fourier-transform rheology. J Condens Matter Phys 2003;15:s923. doi: 10.1088/0953-8984/15/11/316.
[68] Sagis LMC, Ramaekers L, van der Linden E. Constitutive equations for an elastic material with anisotropic rigid particles. Phys Rev E 2001;63:051504. https://doi.org/10.1103/PhysRevE.63.051504.